Mechanism of Particle Size Effect on Electron Injection Efficiency in Ruthenium Dye-Sensitized TiO 2 Nanoparticle Films

ARTICLE *in* THE JOURNAL OF PHYSICAL CHEMISTRY C · MAY 2010

Impact Factor: 4.77 · DOI: 10.1021/jp911418g

5 AUTHORS, INCLUDING:

Luchao Du
National Institute of Advanced Industrial S…
8 PUBLICATIONS **535** CITATIONS
SEE PROFILE

Kohjiro Hara
National Institute of Advanced Industrial S…
154 PUBLICATIONS **11,290** CITATIONS
SEE PROFILE

Mechanism of Particle Size Effect on Electron Injection Efficiency in Ruthenium Dye-Sensitized TiO_2 Nanoparticle Films

Luchao Du, Akihiro Furube,* Kohjiro Hara, Ryuzi Katoh, and M. Tachiya

National Institute of Advanced Industrial Science and Technology (AIST), Tsukuba Central 5, 1-1-1 Higashi, Tsukuba 305-8565, Japan

Received: December 1, 2009; Revised Manuscript Received: April 4, 2010

The kinetics and efficiency of the electron injection process for TiO_2 nanoparticle films composed of different particle sizes ($d = 9$, 20, 30, 50, 169, 200, and 400 nm in diameter) sensitized by N3 dye ($Ru(dcbpy)_2(NCS)_2$) were investigated by using time-resolved fluorescence spectroscopy and femtosecond (transmittance and diffuse reflectance) transient absorption spectroscopy. Different electron injection efficiencies were obtained for different diameter systems. Small diameter systems gave the high electron injection yields, which were around 90%, whereas larger diameter systems gave low efficiencies from 35 to 70%. Judging from the comprehensive and systematic time-resolved spectroscopic data, we concluded that N3 aggregates that formed in spaces between larger diameter TiO_2 nanoparticles were responsible for the low efficiencies.

1. Introduction

Electron transfer dynamics between molecular adsorbates and semiconductor nanoparticles has been the subject of active research for many years because of both applied and fundamental interests.[1,2] In recent years, ultrafast electron injection from dye sensitizer molecules to nanocrystalline semiconductor thin films has been intensely studied by many groups.[3−31] The understanding of these processes is significant to designing and improving Grätzel-type dye-sensitized solar cells, for which charge separation and recombination dynamics play an important role in determining the overall cell efficiency.[32,33] These systems also provide convenient media for studying ultrafast interfacial electron transfer fundamentally.

In such dye-sensitized solar cell (DSSC) systems, usually organic or metal complex dyes are chemically adsorbed on the wide band-gap semiconductor nanoparticles through an anchor group(s) (for example, the carboxyl group) after sinteration of the semiconductor nanoparticle film. The working principle of the initial light-current conversion process in DSSCs is based on the following photophysical and photochemical processes:[15,34,35] Upon photoexcitation of the dye by visible light, electrons are excited from the ground state of the dye to its excited state, and then electron injection occurs from the excited dye into the conduction band of the semiconductor film. The injected electrons relax to the bottom of the conduction band, and then the electrons are trapped in a defect site below the conduction band, followed by diffusion of electrons in the film toward the transparent conductive electrode. The electron injection process must be certain and faster than the competing fluorescence process to achieve a high injection yield. Electron injection is thus a very important primary process in dye-sensitized solar cells.

Wide-gap metal oxide semiconductor nanoparticles have attracted intense interest because of their size-dependent photophysical properties[36−38] and size-dependent performance of DSSCs. TiO_2 is probably the most widely studied material in the field of DSSCs because of its favorable physical/chemical properties, low cost, ease of availability, and high stability. Particle size has a pronounced effect on photon-to-electricity conversion activities in general since it directly affects the specific surface area of semiconductors. As the size of the particle decreases to the nanoscale level, the surface area of the particle increases drastically. There have been some reports that particle size affects electron transport and recombination.[9,22,39−41] By controlling the particle size of the semiconductor, the photophysical and chemical properties can be changed, which, in turn, affect the efficiency of the solar energy conversion for DSSC.

N3 dye (*cis*-bis-(4,4′-dicarboxy-2,2′-bipyridine) dithiocyanato ruthenium(II), or $Ru(dcbpy)_2(NCS)_2$, is one of the best sensitizers for DSSCs, where the N3 dyes adsorb on nanocrystalline TiO_2 film, giving a very high solar-to-electric power conversion efficiency.[42] Nanoscale crystalline TiO_2 films are used to realize a large surface area. Usually about 20 nm diameter TiO_2 nanoparticles are used to make the film, but TiO_2 nanoparticles with diameters of several hundred nanometers are mixed for a better light-harvesting property by multiple light scattering in the film.[43,44] Tachibana et al. found that the appropriate addition of large particles into a transparent ruthenium dye-sensitized TiO_2 film increased the light-harvesting efficiency, but excess addition lowered the light-harvesting efficiency over the visible wavelengths due to enhanced light reflection at the interface between the conducting glass and the TiO_2 film.[45] Their results suggested that an appropriate light-scattering magnitude in the TiO_2 films originating from particle size affected the electron transfer yield as well as the light-harvesting efficiency.

Transient absorption spectroscopy (TAS) is a unique technique to study ultrafast electron injection processes, and the electron injection dynamics in DSSCs was investigated by many groups using femtosecond laser spectroscopy.[4,10−14,16,19,20,25−31,46] Electron injection was found to generally occur within 100 ps,[4,10−13,20,25,29−31] which is much shorter than the excited-state lifetime of typical sensitizer dyes, ensuring the requirement for the high electron injection efficiency. According to the Sundstrom group,[20] electron injection from N3 dye to the conduction band of TiO_2 occurs through two paths, that is, from the initially excited nonthermalized singlet state of the dye and from the

* To whom correspondence should be addressed. E-mail: akihiro-furube@aist.go.jp.

10.1021/jp911418g

thermalized triplet state, accounting for the observed vastly different electron injection times ranging from ~50 fs to ~50 ps. There is a certain difficulty to studying the electron injection yield by using the TAS measurement because it is complicated to determine the absolute concentration of transient species as well as the absorbed photon density.

We have reported that the electron injection efficiency of N3 dye-sensitized 20 nm TiO_2 nanocrystalline film reached almost 100% under visible light (430−650 nm) excitation by using the TAS technique.[9,18,19] Further, Katoh and co-workers found recently that semiconductor size affects electron injection yield in a similar Ru complex dye (called N719)-sensitized TiO_2 system by using time-resolved microwave conductivity measurements.[9] The mechanism, however, is still not clear enough because only two sizes (20 and 300 nm in diameter) were chosen for comparison.

Our present work is to clarify how the TiO_2 particle size affects the electron injection yield. In this study, we examined the electron injection kinetics and efficiency for N3 dye-sensitized TiO_2 systems with different diameters (9, 20, 30, 50, 169, 200, and 400 nm) by means of the time-resolved fluorescence spectroscopy and femtosecond transient absorption spectroscopy. For the transient absorption experiments, IR transmittance and visible/near-IR diffuse reflectance methods were used to measure highly light-scattering films due to the large TiO_2 particles. Systematic experimental results revealed that the electron injection efficiency decreased for larger TiO_2 nanoparticles, which could be attributed to the difference in aggregation states of dye molecules. This study will help in choosing suitable sizes of TiO_2 nanoparticles used in DSSCs.

2. Experimental Section

2.1. Sample Preparation. To make TiO_2 films sensitized homogenously with N3 dye, TiO_2 powders with the following particle diameters were used: 9 nm (pure anatase, ST-01, Ishihara Sangyo, Japan), 20 nm (pure anatase, 95% TiO_2, ST-21, Ishihara Sangyo, Japan), 30 nm (pure anatase, Catalysis Society of Japan, JRC-TIO-13), 50 nm (anatase/rutile, predominantly anatase, Showa Titanium ST series), 169 nm (pure anatase, Merck), 200 nm (pure anatase, ST-41, Ishihara Sangyo, Japan) and 400 nm (anatase/rutile, predominantly anatase, JRC-TIO-2). The technique we used to prepare the films was the doctor blade method. The TiO_2 powder was mixed with water and the organic solvent acetylacetone and ground for 15 min to get the homogeneous mixture. A drop of organic paste mixed with the TiO_2 powder was first put on one side of a glass substrate, and then the paste was spread uniformly using a smooth glass stick with the draw rate around 2 cm/s. The thickness of the TiO_2 film was controlled by adhesive tape (thickness ~ 15 μm) surrounding the square film area. The films were heated at 450 °C for 1 h in O_2 to decompose the organic paste between TiO_2 particles. The N3 dye samples were purchased from Solaronix and Dyesol and were used without purification. To make the N3 solution, the N3 crystal powder was dissolved in a 50:50 (v/v) mixture of *tert*-butyl alcohol (Kanto, G grade) and acetonitrile (Kanto, dehydrated) with a concentration of 0.3 mM. These solvents were used without further purification. N3-sensitized TiO_2 (N3-TiO_2) samples were then prepared by immersing bare TiO_2 films in the N3 dye solution and storing them in the dark for 12 h to ensure the dye molecules sufficiently adsorbed onto the surfaces of the TiO_2 nanoparticles. The N3 dye is adsorbed strongly onto the TiO_2 nanoparticle surface through its carboxyl groups.[47] The films were sufficiently washed with acetone for 24 h to remove the physically absorbed dye and then dried. All operations are done at 25 °C. All the N3-TiO_2 films were 1 cm^2 (1 cm ×1 cm) in area and about 10 μm thick, and they were opaque by light scattering. All the samples were newly prepared before the spectroscopic experiments.

2.2. Femtosecond Diffuse Reflectance and Transmittance Transient Absorption Spectroscopy. To perform transient absorption spectroscopic measurements of such light-scattering films of TiO_2 nanoparticles, we used femtosecond diffuse reflectance transient spectroscopy and measured kinetics and spectra. Some details of femtosecond diffuse reflectance spectroscopy have been described previously regarding the optical setup and performance.[48,49] In this study, the light source for transient diffuse reflectance spectroscopy was a femtosecond titanium sapphire laser with a regenerative amplifier (Hurricane, Spectra Physics, 800 nm, 150 fs, 1 mJ/pulse, 1 kHz). The fundamental output of the laser was divided into two beams. One of the beams was used for pump pulses, and another was used for probe pulses. To obtain a pump light at 532 nm, an 800 nm beam was introduced into an optical parametric amplifier (OPA, TOPAS, Quantronix) with a mixing crystal. The probe beam was obtained by introducing the 800 nm beam into a sapphire plate to generate the white light continuum. The probe beam was further divided into two beams: one beam acted as a reference for compensating the intensity fluctuation of each pulse, another one was irradiated on the sample, and the spectrum of the diffuse reflected light collected by a large lens (50 mm diameter, 80 mm focal length) was detected with a monochromator combined with a photodetector (DET410, Thorlabs) as a function of the probe delay. The pump beam radius on the film surface was about 0.36 mm. Transient absorption intensity is displayed as % absorption given

$$\% \text{ absorption} = 100 \times (1 - R/R_0)$$

where R and R_0 represent the intensities of the diffuse reflected light of the probe pulse with and without excitation, respectively.

IR probe was also used for transient absorption experiments because IR light transmits through thin light-scattering films. For the transmittance transient absorption spectroscopy, we used visible-pump/IR-probe femtosecond transient absorption spectroscopy to observe charge-transfer kinetics by detecting the transient absorption due to injected electrons in the TiO_2 conduction band. Some details of our femtosecond transient absorption spectrometer have been described previously.[12] The fundamental output of the laser was divided into two beams. One of the beams was used for a pump pulse at 550 nm, and another was used for a probe pulse at 3440 nm. The IR probe beam was obtained by introducing the 800 nm beam into another OPA (TOPAS, Quantronix) with a differential frequency generation crystal. The pump and probe lights were overlapped on the film surface, and the transmitted probe light through the sample was collected by a mercury−cadmium−telluride (MCT, Hamamatsu, P3257-10) photodetector. The transient absorption intensity was calculated from the pulse intensity of the probe with and without excitation, typically using thousands of pulses.

2.3. Picosecond Time-Resolved Fluorescence Spectrometer. For time-resolved fluorescence experiments, the excitation light at 532 nm was the same as that used for the transient absorption experiment. Time-resolved fluorescence from the film sample was collected by a streak camera (Hamamatsu, Streak Scope C4334) equipped with a polychromator. The time-resolved fluorescence spectra were recorded with a temporal

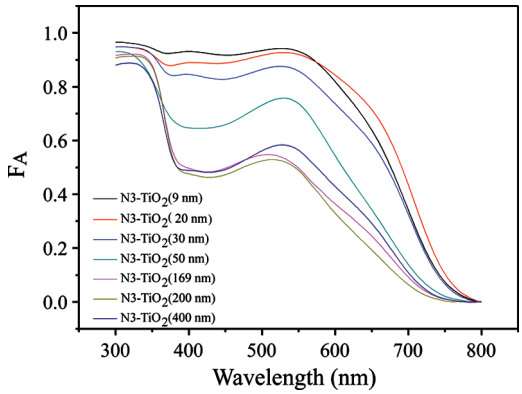

Figure 1. Steady-state absorption fraction spectra of N3-TiO_2. The values in the parentheses indicate the particle diameters of TiO_2.

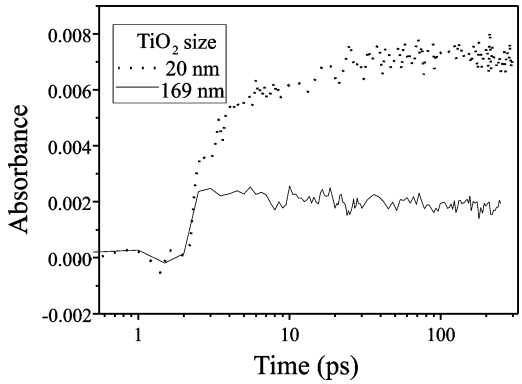

Figure 2. Transient absorption kinetics in N3-TiO_2(20 nm) and N3-TiO_2(169 nm), excited at 550 nm and probed at 3440 nm.

resolution of ~50 ps. All these time-resolved fluorescence and transient absorption measurements were performed at 22 °C.

3. Experimental Results and Discussion

3.1. Steady-State Absorption Spectrum of Different Diameter Systems. Because the samples had strong scattering in the visible light range, a spectrophotometer (Shimadzu, MPC-3100) equipped with an integrating sphere was used to obtain the absorption fraction (F_A) for each sample, as in our previous study.[50] The transmission fraction (F_T) and the reflection fraction (F_R) were measured, and we calculated $F_A = 1 - F_T - F_R$. Figure 1 shows F_A as a function of wavelength for all N3-TiO_2 systems (see the Supporting Information, Figure S1, for details). The absorption band peaks at around 540 nm were known to be metal-to-ligand charge-transfer (MLCT) absorption of N3 dye, in which an electron is transferred from Ru to one of the bipyridine ligands. The peak positions have slight differences for different films. There are many factors that can affect the peak position sensitively.[51] The reason will be explained in the following section compared with results of transient fluorescence spectrum. The F_A values showed differences for different diameter systems. Small diameter systems gave larger F_A's close to 1, whereas large diameter systems gave smaller F_A's. This difference is mainly due to that the larger diameter TiO_2 particles adsorbed smaller numbers of N3 dye molecules because of the smaller specific surface area of the TiO_2 films.

3.2. Particle Size Dependence of Transient Absorption Rise for Injected Electrons in TiO_2. Figure 2 shows the IR transient absorption kinetics of the samples with TiO_2 diameters of 20 and 169 nm (we call them N3-TiO_2(20 nm) and N3-TiO_2(169 nm), respectively). The two kinetics were measured at the same experimental conditions, and the transient absorption amplitudes were corrected by dividing them by the corresponding F_A. We chose to excite at 550 nm (near the MLCT band peak) and probe at 3440 nm, which gives a strong absorption of injected electrons in TiO_2.[50,52] The rise profiles shown in the two kinetics clearly indicated the occurrence of the electron injection process from the excited N3 dye into the conduction band of TiO_2. In Figure 2, we found in N3-TiO_2(20 nm) that the kinetics showed a prompt rise within the time resolution (~250 fs), followed by a slow rise in the ten picosecond time range, then reaching a plateau. On the other hand, in N3-TiO_2(169 nm), the kinetics showed only a fast rise before reaching a plateau with the amplitude much less than that of the N3-TiO_2(20 nm) (~30%). The origin of the slow rise is unclear now and will be discussed later. The ratio of electron injection yield between the two systems is equal to the ratio of the transient absorption intensity in the plateau regions because the amplitude was already corrected by F_A. The electron injection yield of the 20 nm TiO_2 system is around 3 times of that of the 169 nm TiO_2 system. To further confirm the particle size effect on the electron injection yield in these two systems, diffuse reflectance transient absorption kinetics and spectrum measurements were done.

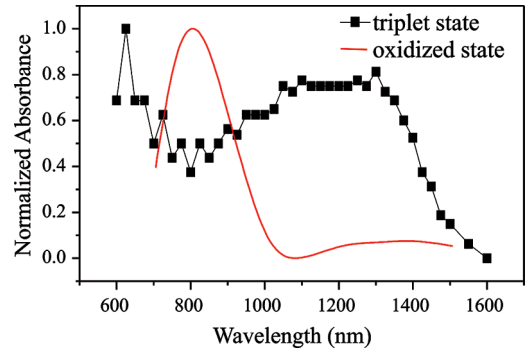

Figure 3. Absorption spectra of the N3 cation (taken from ref 17) and the N3 triplet state (from ref 53).

3.3. Particle Size Effect of Transient Absorption Kinetics and Spectra for N3 Dye. There are already some studies to report transient spectra and kinetics of the N3-TiO_2 system, and G. Benkö et al determined the nature of the triplet state and oxidized state of N3[20] in the wavelength region between 600 and 1050 nm. We have further extended the probe wavelength region. Figure 3 shows the nanosecond absorption spectrum of the oxidized N3 on TiO_2 (taken from ref 17) and N3 triplet state in solution (from ref 53). The formation of the oxidized N3 molecule ($N3^+$) gave absorption at around 810 nm.[17,25,54−58] The band at ~625 nm and the band at longer wavelengths (>900 nm)[10,13,53] are due to the absorption of the triplet state (N3*). The triplet visible peak is close to the cation peak, and it is easy to shift, depending on the protonation condition at the carboxyl groups.[53]

Figure 4a shows the diffuse reflectance transient absorption spectra of N3-TiO_2(20 nm) at 5 and 1000 ps (these times correspond to the kinetics in Figure 4b) under excitation at 532 nm. At 5 ps, transient absorption species of N3* and $N3^+$ are expected to be observed, which overlap each other in the visible/NIR region from 600 to 1000 nm (Figure 3). The ultrafast electron injection process seen in Figure 2 should result in the observation of $N3^+$ with absorption around 810 nm. Also, absorption around 1200 nm is expected because a portion of the electron injection occurs in the later time region. Because of the spectral overlap, it is hard to distinguish N3* and $N3^+$ contributions around 800 nm, whereas the N3* characteristic is clear around 1200 nm. At 1000 ps, the absorption of the triplet

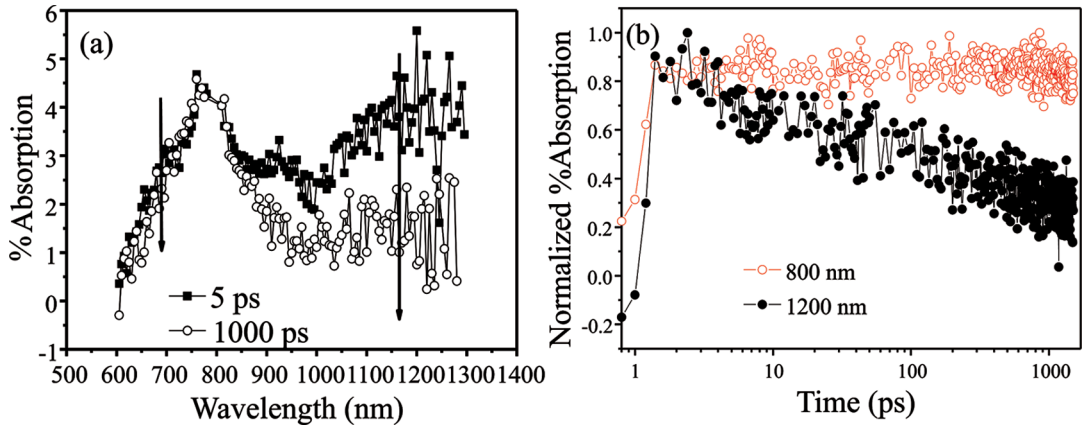

Figure 4. (a) Transient absorption spectra at 5 and 1000 ps for N3-TiO_2(20 nm), excited at 532 nm. (b) Corresponding transient absorption kinetics at 800 and 1200 nm.

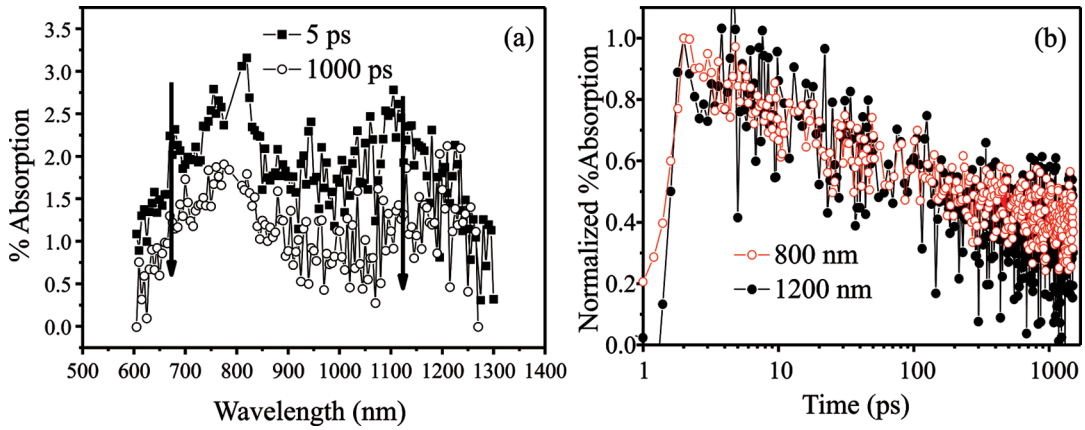

Figure 5. (a) Transient absorption spectra at 5 and 1000 ps for N3-TiO_2(169 nm), excited at 532 nm. (b) Corresponding transient absorption kinetics at 800 and 1200 nm.

state around 1200 nm is weak compared with that at 5 ps, whereas the absorption around 800 nm remains strong and its intensity seems to be the same between 5 and 1000 ps.

Figure 4b shows the normalized transient absorption kinetics for N3-TiO_2(20 nm) at 800 and 1200 nm. The decay kinetics between 800 and 1200 nm shows large differences, agreeing with the temporal spectral change in Figure 4a. Because the transient absorption decay at 1200 nm due to N3* corresponds well to the rise of IR signals in Figure 2, the decay at 1200 nm can be assigned to electron injection from the excited N3 dye to the conduction band of TiO_2. On the other hand, the constant transient species at 800 nm should be the superposition of N3* decay and $N3^+$ rise. The unchanged spectra between 5 and 1000 ps for the spectral range between 600 and 850 nm means that the spectra of N3* and $N3^+$ agreed with each other accidentally for this sample. Similar behavior has been observed for deprotonated N3 dye on TiO_2 by the Sundstrom group.[59]

Figure 5a shows transient absorption spectra at 5 and 1000 ps for N3-TiO_2(169 nm) under the same experimental condition with that of N3-TiO_2(20 nm). The spectral shape does not change with time, and only its amplitude decreases. Judging from the IR kinetics (in Figure 2), which suggested the low efficiency of electron injection, the transient absorption species will be composed of N3* and $N3^+$. The absorption peak at around 1110 nm can be reasonably assigned to N3*, whereas absorption around 800 nm is hard to distinguish again. Figure 5b shows the normalized kinetics at 800 and 1200 nm, which are found to be similar, having a slight slower decay for 800 nm. Also, the 1200 nm kinetics does not agree with the constant IR signals of N3-TiO_2(169 nm) shown in Figure 2, suggesting that the 1200 nm decay must be simply excited-state quenching without participating in electron injection.

Combining the observed spectra and kinetics in two different diameter systems, the electron injection yield of the small diameter system was larger than that of the large diameter system where the excited state seemed to decay without electron injection. The electron injection yields are size-dependent. To obtain the precise value of the electron injection yield and clarify the mechanism, we performed a systematic experiment for a series of different diameter systems by using time-resolved fluorescence spectroscopy because time-resolved fluorescence is generally more sensitive and accurate than transient absorption, and therefore, this is more suitable for systematic experiments for a lot of samples.

3.4. Time-Resolved Fluorescence for a Series of Different Diameter Systems. To clarify the electron injection mechanism, the transient emission kinetics (Figure 6a) of N3-TiO_2 for all different TiO_2 diameters as well as of N3 solution and powder were measured. The 610−839 nm spectral region was integrated to get these decay curves. All the emission intensities from the N3-TiO_2 samples were corrected by the corresponding F_A, and the emission intensities of the N3 solution and powder were normalized at a fix value (the details shown later). From Figure 6a, different emission intensities and kinetics are clearly shown for different diameter TiO_2 systems. For smaller systems (9, 20, 30, and 50 nm TiO_2), the weak intensities at time zero, followed by faster decay, were observed, ensuring the high electron injection yield. On the other hand, the high emission intensity, followed by slower decay, on the N3-TiO_2(169 nm) system was observed, clearly indicating the lower electron

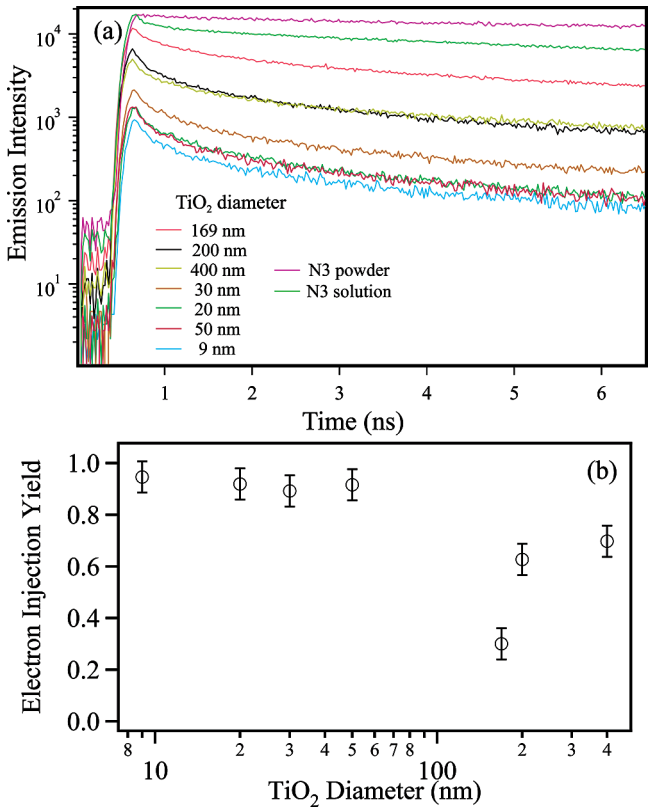

Figure 6. (a) Fluorescence kinetics of different N3-TiO_2 systems, N3 solution, and N3 powder, all excited at 500 nm. (b) Electron injection yield of all the samples as a function of TiO_2 diameter.

injection efficiency, and the emission lifetime in the later time region (>2 ns) actually seems nearly the same as that of N3 solution. This fact indicates that many excited N3 dyes remained without participating electron injection. A high emission intensity, followed by the slower decay, was also shown in 200 and 400 nm TiO_2 systems, indicating, again, the lower electron injection yields. The emission lifetime of N3 powder is slower than that of N3 solution.

The results in Figure 2 with the plateaus after ~50 ps ensured that electron injection occurs dominantly within the time-resolution of the streak camera (~50 ps). The Supporting Information (Figure S2) also ensures this for other N3-TiO_2 samples. Compared with the experimental curves shown in Figure 2, where the IR transient absorption kinetics are characteristics of the injected electrons, the ratio of electron injection yield between the 20 and 169 nm TiO_2 systems calculated from Figure 2 should be equal to the ratio of the fluorescence emission quenching just after excitation of these two systems calculated from Figure 6a. The emission intensity just after excitation of the "no quenching" reference can then be obtained, which gave the value of 16 800. The intensities of the N3 solution and power samples were normalized to this value for easy comparison on the figure. Thus, the electron injection yields of all the different systems can be calculated using the ratio of the fluorescence emission intensity just after excitation to the value of 16 800. The electron injection yields of 9, 20, 30, 50, 169, 200, and 400 nm diameter systems are 95, 92, 89, 92, 30, 63 and 70%, respectively, as shown in Figure 6b. The calculated results showed that the smaller diameter systems gave the high electron injection yield that is larger than 89%, whereas the larger ones gave relatively low efficiencies around 70%. Surprisingly, the 169 nm diameter system gave an extremely low electron injection yield that is only 30%.

We used the double exponential function to fit the decay curves after the dominant electron injection in Figure 6a, and the results are shown in Table 1. Here, τ_1 represents the fast decay time constant, and τ_2 represents the slow one. A_1 and A_2 are the ratios of the fast and slow components to the maximum amplitude, respectively. From the fitting results, the time constants of the fast time constants have no large difference for all N3-TiO_2 systems ranging between 0.13 and 0.22 ns. Furthermore, a similar time constant (0.17 ns) is seen for the N3 solution. Also, the slow time constants are between 1.4 and 2.3 ns for all N3-TiO_2 systems, which are several times shorter than those for solution and power samples (6 and 12 ns, respectively). That these decay processes in N3-TiO_2 are faster than the references (solution and powder) can be due to the minor contribution of electron injection and/or some other quenching processes of the triplet state. According to the discussion of Figures 2, 4a,b, and 5a,b, for the small diameter systems, the fast reaction component is likely due to the minor electron injection, and for the large diameter systems, the fast reaction component is likely due to some other quick relaxation of the triplet state.

From the fluorescence spectral shape, we can discuss the property of N3 dye that could not inject an electron into TiO_2. Figure 7a shows the normalized time-integrated fluorescence spectra of all N3-TiO_2 systems, N3 powder, and N3 solution. The result shows that the peak positions of larger diameter systems have blue shifted compared with that of small diameter systems (Figure 7b). The trend of peak shift in Figure 7a,b matched with that in absorption shown in Figure 1. Compared with the peak positions between N3 powder and N3 solution, there is a large blue shift for N3 powder.

According to Nazzeruddin et al.,[51] the shift of absorption peak of N3 dye is very sensitive to pH, and protonation at the carboxyl groups leads to a red shift.[51] The dye molecules in our solution and on TiO_2 should have the deprotonated form because, otherwise, dye absorption does not occur. There would then be a red shift of the peak position of N3 if N3 dye

TABLE 1: Decay Time and Fitting Parameters of the Transient Fluorescence

	fitting parameter			
TiO_2 diameter (nm)	τ_1 (ns)	τ_2 (ns)	A_1	A_2
9	0.18 ± 0.01	1.6 ± 0.1	58 ± 1%	42 ± 1%
20	0.13 ± 0.01	1.4 ± 0.1	49 ± 1%	51 ± 1%
30	0.19 ± 0.01	1.6 ± 0.1	54 ± 1%	46 ± 1%
50	0.18 ± 0.01	1.6 ± 0.1	61 ± 2%	39 ± 2%
169	0.22 ± 0.01	2.3 ± 0.1	45 ± 1%	55 ± 1%
200	0.16 ± 0.01	1.6 ± 0.1	56 ± 1%	44 ± 1%
400	0.16 ± 0.01	1.7 ± 0.1	50 ± 1%	51 ± 1%
N3 solution	0.17 ± 0.01	6 ± 0.2	37 ± 1%	63 ± 1%
N3 powder	1.4 ± 0.9	12 ± 10	15 ± 10%	85 ± 30%

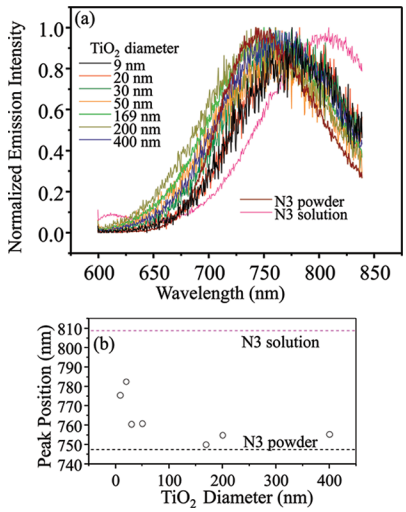

Figure 7. (a) Normalized time-integrated fluorescence spectra of different diameter N3-TiO_2 systems, N3 powder, and N3 solution, measured by a streak camera after excitation at 500 nm. (b) The graph plots the peak position of the fluorescence spectrum for different diameter TiO_2 systems. The red dashed line is the peak position of N3 solution, whereas the black dashed line is the peak position of N3 powder.

molecules become crystal with the neutral (protonated) form. The observed blue shift in the crystal form (N3 powder) will not be due to the difference of proton number but due to molecular interaction. Such aggregation will be a possible reason why the peak positions of larger diameter systems have blue shifted compared with that of small diameter systems, and resultantly, it would give lower electron injection efficiency.

3.5. Models to Explain the Particle Size Dependence of Electron Injection Yield. Two possible mechanisms can be raised regarding the difference in the obtained electron injection yield for different diameter systems. One is the aggregation formation, as mentioned above, and the other is the surface state difference.

Nanosized semiconductor particles exhibit pronounced size effects on electronic structure and related optical properties. As the size of the semiconductor crystal changes, different facets and surface steps may be created. These different surface species induced by different diameters are expected to have varied electron injection capabilities. Small TiO_2 nanoparticles have a high surface area/volume ratio, which gives rise to a lot of defects. Different diameter TiO_2 may have different defect densities on the surface. Note that the TiO_2 quantum size effect, that is, the exciton confinement effect, appears only at a diameter of less than 1.5 nm, so the quantum effect is not likely in our case because the diameter of TiO_2 is larger than 9 nm in our study.[60]

According to the Marcus electron-transfer theory[61] and its modified form for dye-sensitized semiconductors,[3] the density of states in the semiconductor coupled to the adsorbate affects the electron injection rate. The density of electron acceptor states is composed of the conduction band having the $E^{1/2}$ shape and a tail (which is named "defect") below the conduction-band edge due to surface trap states. A change of surface state can cause a change of acceptor state density. The different contributions of electron injection into surface states can induce different electron injection efficiencies.

It is known that adsorption of ions or molecules to the surface of a semiconductor can induce a change in the flat band potential level.[62] In DSSCs, adsorption-induced shifts in the band edges are expected to be significant for the high surface area nanocrystalline TiO_2 semiconductor thin films. It has also been reported that a remarkable cation-dependent shift occurred in the flat band potential of TiO_2 with Li^+ adsorption.[11,63] A positive shift in the density of TiO_2 conduction/trap states in the presence of Li^+ ions can increase the possibility of electron injection occurrence because the electron acceptor density for the excited sensitizer dye can increase due to the conduction band shifting positively. Namely, a larger TiO_2 density of states at a fixed electron donor level (the LUMO of N3* dye) is expected to increase the electron injection rate and yield from the triplet state of the dye (Figure 8a).

As we know, dye aggregation is not good for achieving high performance of DSSCs. In general, aggregation can change the nature of the excited state of organic molecules. Our previous study on perylene revealed that a change in the aggregation manner from the monomer in solution to dimeric crystal led to stabilization of the lowest singlet excited state.[64] This kind of stabilization effect of an electron donor would be energetically unfavorable for efficient electron injection. In the case of N3 dye, aggregation seems to unstabilize the excited state (triplet state) slightly, judging from the blue shift of the emission spectrum of the power sample by ~0.1 eV compared with the solution sample (Figure 7). This energy change should be favorable for an electron donor, but the far distance between the molecules in the aggregate and the TiO_2 surface should decreases drastically the possibility of electron transfer. Actually, exciton diffusion lengths in organic solids are usually only a few tens of nanometers or less.[65,66] For electron injection, excitons must move to the aggregate/TiO_2 contacting point where the electronic coupling is strong; however, this possibility should be very small because of random diffusion of excitons.

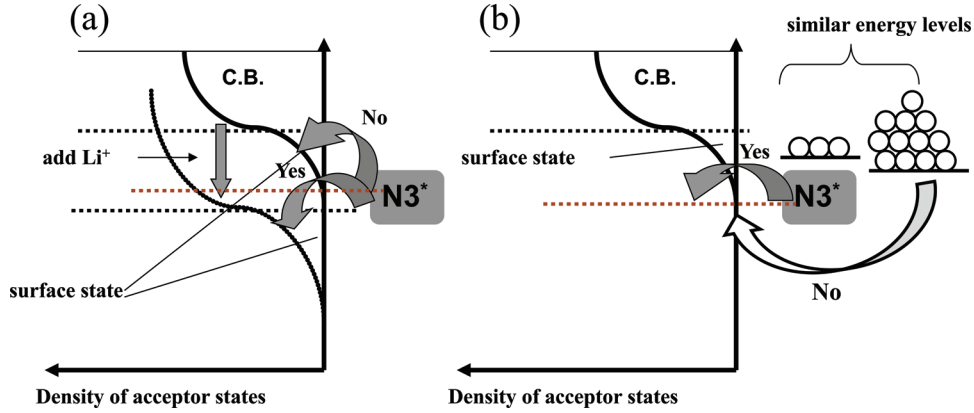

Figure 8. Schematic energy diagrams of N3-TiO_2 systems, which can be affected by Li^+ ions (a) and aggregation of N3 molecules (b).

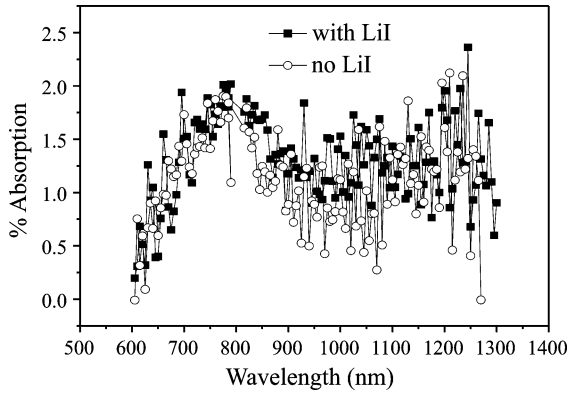

Figure 9. Femtosecond transient absorption spectra for N3-TiO_2(169 nm) without and with Li^+ ions at 1000 ps after 532 nm excitation.

Because aggregation does not change the potential level of the semiconductor and hardly does that of excited N3, the aggregation effect appears as an inactive electron donor, which only loses the photon energy through relaxation within the aggregate (Figure 8b). In the following section, we will discuss in detail the above two possibilities.

3.5.1. Surface State Effect. Different diameter TiO_2 will have different surface states; the surface defect density may be smaller for larger diameter systems, which might make the electron injection yield smaller. To check if there is the surface state effect or not, the effect of Li^+ was applied to change the surface property of TiO_2 in the N3-TiO_2(169 nm) system. Li^+ ions are known to be potential-determining ions for semiconductor conduction[11,63,67] and valence bands when they exist in a dye-sensitized semiconductor film. After adsorption of the positive Li^+ ions on the TiO_2 surface and intercalation of the ions into the TiO_2 lattice,[63,67−69] the electrochemical potential of TiO_2 undergoes a positive shift. The shift around 0.4−1 eV[11,70] will produce a large effect for electron injection yield because of a larger potential difference from the conduction-band edge to the LUMO level of the dye.[68−70]

Figure 9 shows the femtosecond diffuse reflectance transient absorption spectra for N3-TiO_2 (169 nm) without and with Li^+ ions at 1000 ps after excitation at 532 nm. A solution of 0.1 mol/L LiI in acetonitrile was added to cover the film. There is little difference in the spectra dominated by the triplet state of N3 before and after adding Li^+. If the surface state effect does work for the low electron injection yield that was observed above, the electron injection yield here should be increased a lot by the Li^+ effect. The experimental results showed that a change in the conduction band level by Li^+ has no effect on the electron injection yield in the 169 nm sample, which indicated that the different surface state was not the reason for the low electron injection yields in the larger TiO_2 diameter systems.

3.5.2. Aggregation for Different Diameter Systems. There are many studies related to N3 aggregation in DSSCs.[71−73] There are also reports that large N3 aggregates can form on the surface of ZnO films, which suppressed electron injection.[14,73] Actually, even small aggregates, such as H dimers, can decrease the electron injection efficiency for a merocyanine dye.[72] Murai et al. found that the aggregation of N3 occurred on ZrO_2 nanocrystalline film, and it affected the peak position of absorption bands of the triplet state and the ground state of N3 dye.[53] Aggregation may have the largest possibility to affect the injection yield. To clarify aggregation effects, examining the condition of the aggregate state on the surface is important.

TABLE 2: Calculation Results of N3 Dye Coverage on the TiO_2 Surface for all N3-TiO_2 Systems

TiO_2 diameter (nm)	number of N3 dye coverage
9	0.1
20	0.45
30	0.36
50	0.46
169	2
200	3.4
400	2.4

For different diameter TiO_2 systems, the surface property of TiO_2 varies from each other. The larger diameter TiO_2 have the smaller specific surface area, resulting in the poor chemical adsorption of the dye molecules. Also, the gap between two TiO_2 nanoparticles is broader than that of the smaller diameter systems, where enough space for physical adsorption of more N3 dye can be provided, increasing the possibility of dye aggregation.

From the steady-state absorption spectrum of N3 dye absorbed on the TiO_2 surface, we estimated the density of N3 dye in the TiO_2 film using the Beer's law to judge if dye aggregates existed in the space between nanoparticles. The absorption fraction values of Figure 1 were converted to optical densities. Using the absorption coefficient[74] at 500 nm, which is 1.18×10^4 dm^3 mol^{-1} cm^{-1} and the surface area of each TiO_2 nanoparticle from the data sheet of powers, we calculated the N3 dye coverage on the surface of TiO_2. Because the molecular size of N3 dye[75,76] is about 1 nm^2, we define the coverage to be 1 when the number of N3 molecules per surface area in the film is 1 nm^{-1}. The calculation results are shown in Table 2. Submonolayer coverages of N3 dye were found in the smaller diameter systems (from 9 to 50 nm), whereas more than a monolayer was estimated for the larger diameter systems, suggesting the aggregation of N3 dye. It should be noted that, to estimate the number N3 molecules using the Beer's law, we introduce an assumption that the incident light can go straight through the film. For small diameter samples, the assumption is reasonable because there is weak scattering of the films, but for the larger diameter systems, the propagation length of the light in the film should be shorter than the film thickness because of the efficient backscattering near the film surface. This, however, does not affect our conclusion because the real value of N3 dye coverage will become larger, which further supports the idea of aggregation.

Combining the results shown in Table 2 with all the experimental results mentioned above, we can confirm that the aggregation of N3 dye in the larger diameter systems is responsible for the low electron injection yield.

3.6. Origin of the Slow Injection in the 20 and 30 nm Diameter Systems. Recently, there have been many studies discussing the slow injection dynamics on the picosecond time scale on N3 (or similar N719) sensitized TiO_2 nanocrystalline films. The slow electron transfer occurs from the thermalized triplet state and is characterized by a multiexponential function in the 1−100 ps range.[4,20,21,25] The origin of the multiexponentiality of the triplet injection has been assigned to the heterogeneity of the conduction band energy[77] by Tachibana et al., triplet state energies[24] and interligand electron transfer within the sensitizer[23] by the Sundstrom group, and variation in electron transfer couplings by the Lian group.[4] The slow picosecond injection phase was suggested by Moser et al. to be due to aggregation of the sensitizer on the semiconductor surface.[78] Contrarily, only picosecond time scale injection was reported by Durrant and co-workers.[79] Most recently, slow electron

injection was observed in monolayer dye-sensitized TiO_2 by the Sundstrom group.[59]

In our case, the slow rise was found only in the small diameter systems of 20 and 30 nm (Figure 2 and the Supporting Information, Figure S2), but this feature was not seen for all the small diameter systems. Slow injection dynamics was not found in 9 and 50 nm and also larger diameter systems. We propose that there are some possibilities: one is different surface defects in different diameter systems, which may affect the electron injection time, and another is the different crystallinity in different diameter systems to induce the different surface structure, which made the electron injection time different. There is also a possibility that the purity of TiO_2 powder has an effect on the electron injection time. The origin of the slow injection will be not only one, but many factors can reduce the interaction between the triplet state and TiO_2 surface compared with that between the excited singlet state and the TiO_2 surface. In the case of the black dye, even the solvent changed the appearance of such slow injection processes, and the origin was assigned to solvation of the charge separated state.[17] More studies will be necessary to understand the origin of slow injection.

4. Conclusion

We used time-resolved fluorescence and transient absorption spectroscopy to systematically study the electron injection and excited-state decay kinetics for different diameter TiO_2 particles ($d = 9$, 20, 30, 50, 169, 200, and 400 nm in diameter) sensitized by N3 dye. Electron injection efficiencies were found to be strongly dependent on the diameter of the TiO_2 particle. High electron injection yields, around 90%, were found in smaller diameter systems ($d \leq 50$ nm), whereas other larger particles gave low efficiencies around 30−70%. The N3 dye coverage of the larger diameter systems was larger than that of small diameter systems and more than a monolayer, which resulted in the low efficiency in the larger diameter systems. Judging from the time-resolved fluorescence spectra and an experiment using potential-controlling Li^+ ions, it was found that N3 aggregates that formed in spaces between TiO_2 nanoparticles were the most major factor lowering the electron injection efficiency rather than the size-dependent surface nature of TiO_2. For DSSC application, dye aggregation must be carefully treated and avoided to achieve high performance, especially when using larger semiconductor nanoparticles, which often work as a light-scattering material.

Acknowledgment. We thank Prof. B. Ohtani and Prof. R. Abe at Hokkaido University for their kind help in supplying us with 30, 50, 169, and 400 nm TiO_2 powders.

Supporting Information Available: Details on the absorption fraction measurement and the IR transient absorption kinetics. This material is available free of charge via the Internet at http://pubs.acs.org.

References and Notes

(1) Hagfeldt, A.; Grätzel, M. *Chem. Rev.* **1995**, *95*, 49.
(2) Kamat, P. V., Meisel, D., Eds. *Semiconductor Nanoclusters - Physical, Chemical and Catalytic Aspects*; Elsevier Science: Amsterdam, 1997.
(3) Asbury, J. B.; Hao, E.; Wang, Y. Q.; Ghosh, H. N.; Lian, T. Q. *J. Phys. Chem. B* **2001**, *105*, 4545.
(4) Asbury, J. B.; Anderson, N. A.; Hao, E.; Ai, X.; Lian, T. *J. Phys. Chem. B* **2003**, *107*, 7376.
(5) Asbury, J. B.; Wang, Y. Q.; Hao, E. C.; Ghosh, H. N.; Lian, T. *Res. Chem. Intermed.* **2001**, *27*, 315.
(6) Asbury, J. B.; Ellingson, R. J.; Ghosh, H. N.; Ferrere, S.; Nozik, A. J.; Lian, T. *J. Phys. Chem. B* **1999**, *103*, 3110.
(7) Ellingson, R. J.; Asbury, J. B.; Ferrere, S.; Ghosh, H. N.; Sprague, J. R.; Lian, T.; Nozik, A. J. *J. Phys. Chem. B* **1998**, *102*, 6455.
(8) Anderson, N. A.; Hao, E.; Ai, X.; Hastings, G.; Lian, T. *Chem. Phys. Lett.* **2001**, *347*, 304.
(9) Katoh, R.; Huijser, A.; Hara, K.; Savenije, T. J.; Siebbeles, L. D. A. *J. Phys. Chem. C* **2007**, *111*, 10741.
(10) Furube, A.; Katoh, R.; Hara, K.; Murata, S.; Arakawa, H.; Tachiya, M. *J. Phys. Chem. B* **2003**, *107*, 4162.
(11) Furube, A.; Katoh, R.; Hara, K.; Sato, T.; Murata, S.; Arakawa, H.; Tachiya, M. *J. Phys. Chem. B* **2005**, *109*, 16406.
(12) Furube, A.; Katoh, R.; Yoshihara, T.; Hara, K.; Murata, S.; Arakawa, H.; Tachiya, M. *J. Phys. Chem. B* **2004**, *108*, 12583.
(13) Furube, A.; Murai, M.; Watanabe, S.; Hara, K.; Katoh, R.; Tachiya, M. *J. Photochem. Photobiol., A* **2006**, *182*, 273.
(14) Horiuchi, H.; Katoh, R.; Hara, K.; Yanagida, M.; Murata, S.; Arakawa, H.; Tachiya, M. *J. Phys. Chem. B* **2003**, *107*, 2570.
(15) Katoh, R.; Furube, A.; Barzykin, A. V.; Arakawa, H.; Tachiya, M. *Coord. Chem. Rev.* **2004**, *248*, 1195.
(16) Katoh, R.; Furube, A.; Hara, K.; Murata, S.; Sugihara, H.; Arakawa, H.; Tachiya, M. *J. Phys. Chem. B* **2002**, *106*, 12957.
(17) Katoh, R.; Furube, A.; Kasuya, M.; Fuke, N.; Koide, N.; Han, L. *J. Mater. Chem.* **2007**, *17*, 3190.
(18) Katoh, R.; Furube, A.; Murai, M.; Tamaki, Y.; Hara, K.; Tachiya, M. *C. R. Chim.* **2006**, *9*, 639.
(19) Katoh, R.; Furube, A.; Yoshihara, T.; Hara, K.; Fujihashi, G.; Takano, S.; Murata, S.; Arakawa, H.; Tachiya, M. *J. Phys. Chem. B* **2004**, *108*, 4818.
(20) Benko, G.; Kallioinen, J.; Korppi-Tommola, J. E. I.; Yartsev, A. P.; Sundström, V. *J. Am. Chem. Soc.* **2002**, *124*, 489.
(21) Kallioinen, J.; Benko, G.; Sundström, V.; Korppi-Tommola, J. E. I.; Yartsev, A. P. *J. Phys. Chem. B* **2002**, *106*, 4396.
(22) Benko, G.; Skarman, B.; Wallenberg, R.; Hagfeldt, A.; Sundström, V.; Yartsev, A. P. *J. Phys. Chem. B* **2003**, *107*, 1370.
(23) Benko, G.; Kallioinen, J.; Myllyperkio, P.; Trif, F.; Korppi-Tommola, J. E. I.; Yartsev, A. P.; Sundström, V. *J. Phys. Chem. B* **2004**, *108*, 2862.
(24) Myllyperkio, P.; Benko, G.; Korppi-Tommola, J.; Yartsev, A. P.; Sundström, V. *Phys. Chem. Chem. Phys.* **2008**, *10*, 996.
(25) Tachibana, Y.; Moser, J. E.; Grätzel, M.; Klug, D. R.; Durrant, J. R. *J. Phys. Chem.* **1996**, *100*, 20056.
(26) Heimer, T. A.; Heilweil, E. J.; Bignozzi, C. A.; Meyer, G. J. *J. Phys. Chem. A* **2000**, *104*, 4256.
(27) Bergeron, B. V.; Kelly, C. A.; Meyer, G. J. *Langmuir* **2003**, *19*, 8389.
(28) Kelly, C. A.; Meyer, G. J. *Coord. Chem. Rev.* **2001**, *211*, 295.
(29) Haque, S. A.; Palomares, E.; Cho, B. M.; Green, A. N. M.; Hirata, N.; Klug, D. R.; Durrant, J. R. *J. Am. Chem. Soc.* **2005**, *127*, 3456.
(30) Huber, R.; Sporlein, S.; Moser, J. E.; Grätzel, M.; Wachtveitl, J. *J. Phys. Chem. B* **2000**, *104*, 8995.
(31) Bauer, C.; Boschloo, G.; Mukhtar, E.; Hagfeldt, A. *J. Phys. Chem. B* **2001**, *105*, 5585.
(32) O'Regan, B.; Grätzel, M. *Nature* **1991**, *353*, 737.
(33) Bach, U.; Lupo, D.; Comte, P.; Moser, J. E.; Weissortel, F.; Salbeck, J.; Spreitzer, H.; Grätzel, M. *Nature* **1998**, *395*, 583.
(34) Durrant, J. R.; Haque, S. A.; Palomares, E. *Chem. Commun.* **2006**, 3279.
(35) Hara, K.; Horiuchi, H.; Katoh, R.; Singh, L. P.; Sugihara, H.; Sayama, K.; Murata, S.; Tachiya, M.; Arakawa, H. *J. Phys. Chem. B* **2002**, *106*, 374.
(36) Alivisatos, A. P. *Science* **1996**, *271*, 933.
(37) Henglein, A. *Chem. Rev.* **1989**, *89*, 1861.
(38) Micic, O. I.; Nozik, A. J. *J. Lumin.* **1996**, *70*, 95.
(39) Hao, Y.-Q.; Wang, Y.-F.; Weng, Y.-X. *J. Phys. Chem. C* **2008**, *112*, 8995.
(40) Cass, M. J.; Walker, A. B.; Martinez, D.; Peter, L. M. *J. Phys. Chem. B* **2005**, *109*, 5100.
(41) Zhu, K.; Kopidakis, N.; Neale, N. R.; van de Lagemaat, J.; Frank, A. J. *J. Phys. Chem. B* **2006**, *110*, 25174.
(42) Nazeeruddin, M. K.; Kay, A.; Rodicio, I.; Humphry-Baker, R.; Mueller, E.; Liska, P.; Vlachopoulos, N.; Grätzel, M. *J. Am. Chem. Soc.* **1993**, *115*, 6382.
(43) Wang, Z.-S.; Kawauchi, H.; Kashima, T.; Arakawa, H. *Coord. Chem. Rev.* **2004**, *248*, 1381.
(44) Hore, S.; Vetter, C.; Kern, R.; Smit, H.; Hinsch, A. *Sol. Energy Mater. Sol. Cells* **2006**, *90*, 1176.
(45) Tachibana, Y.; Hara, K.; Sayama, K.; Arakawa, H. *Chem. Mater.* **2002**, *14*, 2527.
(46) Yoshihara, T.; Katoh, R.; Furube, A.; Murai, M.; Tamaki, Y.; Hara, K.; Murata, S.; Arakawa, H.; Tachiya, M. *J. Phys. Chem. B* **2004**, *108*, 2643.

(47) Nazeeruddin, M. K.; Humphry-Baker, R.; Liska, P.; Grätzel, M. *J. Phys. Chem. B* **2003**, *107*, 8981.
(48) Asahi, T.; Furube, A.; Fukumura, H.; Ichikawa, M.; Masuhara, H. *Rev. Sci. Instrum.* **1998**, *69*, 361.
(49) Furube, A.; Asahi, T.; Masuhara, H.; Yamashita, H.; Anpo, M. *J. Phys. Chem. B* **1999**, *103*, 3120.
(50) Du, L. C.; Furube, A.; Yamamoto, K.; Hara, K.; Katoh, R.; Tachiya, M. *J. Phys. Chem. C* **2009**, *113*, 6454.
(51) Nazeeruddin, M. K.; Zakeeruddin, S. M.; Humphry-Baker, R.; Jirousek, M.; Liska, P.; Vlachopoulos, N.; Shklover, V.; Fischer, C.-H.; Grätzel, M. *Inorg. Chem.* **1999**, *38*, 6298.
(52) Yoshihara, T.; Katoh, R.; Furube, A.; Tamaki, Y.; Murai, M.; Hara, K.; Murata, S.; Arakawa, H.; Tachiya, M. *J. Phys. Chem. B* **2004**, *108*, 3817.
(53) Murai, M.; Furube, A.; Yanagida, M.; Hara, K.; Katoh, R. *Chem. Phys. Lett.* **2006**, *423*, 417.
(54) Tachibana, Y.; Haque, S. A.; Mercer, I. P.; Durrant, J. R.; Klug, D. R. *J. Phys. Chem. B* **2000**, *104*, 1198.
(55) Kallioinen, J.; Lehtovuori, V.; Myllyperkiö, P.; Korppi-Tommola, J. *Chem. Phys. Lett.* **2001**, *340*, 217.
(56) Moser, J. E.; Noukakis, D.; Bach, U.; Tachibana, Y.; Klug, D. R.; Durrant, J. R.; Humphry-Baker, R.; Grätzel, M. *J. Phys. Chem. B* **1998**, *102*, 3649.
(57) Das, S.; Kamat, P. V. *J. Phys. Chem. B* **1998**, *102*, 8954.
(58) Kuciauskas, D.; Freund, M. S.; Gray, H. B.; Winkler, J. R.; Lewis, N. S. *J. Phys. Chem. B* **2001**, *105*, 392.
(59) Pellnor, M.; Myllyperkiö, P.; Korppi-Tommola, J.; Yartsev, A.; Sundström, V. *Chem. Phys. Lett.* **2008**, *462*, 205.
(60) Monticone, S.; Tufeu, R.; Kanaev, A. V.; Scolan, E.; Sanchez, C. *Appl. Surf. Sci.* **2000**, *162−163*, 565.
(61) Gosavi, S.; Marcus, R. A. *J. Phys. Chem. B* **2000**, *104*, 2067.
(62) Vandermolen, J.; Gomes, W. P.; Cardon, F. *J. Electrochem. Soc.* **1980**, *127*, 324.
(63) Redmond, G.; Fitzmaurice, D. *J. Phys. Chem.* **1993**, *97*, 1426.
(64) Furube, A.; Murai, M.; Tamaki, Y.; Watanabe, S.; Katoh, R. *J. Phys. Chem. A* **2006**, *110*, 6465.
(65) Watanabe, S.; Furube, A.; Katoh, R. *J. Phys. Chem. A* **2006**, *110*, 10173.
(66) Yago, T.; Tamaki, Y.; Furube, A.; Katoh, R. *Phys. Chem. Chem. Phys.* **2008**, *10*, 4435.
(67) Boschloo, G.; Fitzmaurice, D. *J. Phys. Chem. B* **1999**, *103*, 7860.
(68) Watson, D. F.; Meyer, G. J. *Coord. Chem. Rev.* **2004**, *248*, 1391.
(69) Kelly, C. A.; Farzad, F.; Thompson, D. W.; Stipkala, J. M.; Meyer, G. J. *Langmuir* **1999**, *15*, 7047.
(70) Tachibana, Y.; Haque, S. A.; Mercer, I. P.; Moser, J. E.; Klug, D. R.; Durrant, J. R. *J. Phys. Chem. B* **2001**, *105*, 7424.
(71) Kambe, S.; Murakoshi, K.; Kitamura, T.; Wada, Y.; Yanagida, S.; Kominami, H.; Kera, Y. *Sol. Energy Mater. Sol. Cells* **2000**, *61*, 427.
(72) Khazraji, A. C.; Hotchandani, S.; Das, S.; Kamat, P. V. *J. Phys. Chem. B* **1999**, *103*, 4693.
(73) Keis, K.; Lindgren, J.; Lindquist, S.-E.; Hagfeldt, A. *Langmuir* **2000**, *16*, 4688.
(74) Karuppuchamy, S.; Nonomura, K.; Yoshida, T.; Sugiura, T.; Minoura, H. *Solid State Ionics* **2002**, *151*, 19.
(75) Sasahara, A.; Pang, C. L.; Onishi, H. *J. Phys. Chem. B* **2006**, *110*, 4751.
(76) Shklover, V.; Ovchinnikov, Y. E.; Braginsky, L. S.; Zakeeruddin, S. M.; Grätzel, M. *Chem. Mater.* **1998**, *10*, 2533.
(77) Tachibana, Y.; Rubtsov, I. V.; Montanari, I.; Yoshihara, K.; Klug, D. R.; Durrant, J. R. *J. Photochem. Photobiol., A* **2001**, *142*, 215.
(78) Wenger, B.; Grätzel, M.; Moser, J.-E. *J. Am. Chem. Soc.* **2005**, *127*, 12150.
(79) Tachibana, Y.; Nazeeruddin, M. K.; Grätzel, M.; Klug, D. R.; Durrant, J. R. *Chem. Phys.* **2002**, *285*, 127.

JP911418G